Supporting Online Material for

4D Electron Diffraction Reveals Correlated Unidirectional Behavior in Zinc Oxide Nanowires

Ding-Shyue Yang, Changshi Lao, Ahmed H. Zewail*

*To whom correspondence should be addressed. E-mail: Zewail@caltech.edu

Published 19 September 2008, *Science* **321**, 1660 (2008)
DOI: 10.1126/science.1162049

This PDF file includes:

Materials and Methods
Figs. S1 to S3
References

Supporting Online Material

4D Electron Diffraction Reveals Unidirectional Correlated Behavior in ZnO Nanowires

Ding-Shyue Yang, Changshi Lao and Ahmed H. Zewail*

Materials and methods

Ultrafast electron crystallography (UEC) as a method for studying crystalline structures, surfaces and nanometer-scale interfaces, with atomic-scale spatial and femtosecond temporal resolutions, has been described in detail elsewhere (*S1*, *S2*). Our apparatus integrates a femtosecond laser system into an ultrahigh vacuum chamber assembly (Fig. S1). Basically, the output of Ti:sapphire femtosecond laser (with a pulse width of 120 fs) is split into two beams: an 800 nm pulse which is used to excite the sample and a 266 nm pulse (generated by frequency tripling) to produce an electron packet via the photoelectric effect. The electrons are then accelerated at 30 kV resulting in a de Broglie wavelength of $\lambda = 0.07$ Å; the electron beam has a diameter of ~200 μm on the screen. The diffraction patterns of these electrons from the sample are recorded on a charge-coupled device (CCD) camera with single-electron sensitivity. The delay time between the initiating laser pulse and electron probe packet is varied by changing the optical path length between the two pulses. Diffraction patterns at different delay times (diffraction frames) provide a movie of structural change (Fig. S2A) (*S1*).

Observation of reflection Bragg diffractions from the material is achieved with electron packets incident at near grazing angles. As a result, the electron beam has a footprint of a few mm by 0.2 mm on the surface of the material. Because the speed of electrons is about one-third that of light, a large group velocity mismatch occurs between the laser pulse and the electron packet. In order to resolve this issue and achieve an ultrashort temporal resolution, we have implemented a wavefront tilting scheme so that the laser pulse arrives at every point on the sample precisely at the same time as the electron packet (*S2*–*S4*). All time-resolved experiments reported here used this “tilted geometry,” with the laser pulse vertically incident on the specimen (Fig. S1).

The samples were supported on a high-precision goniometer with three degrees of freedom in translation and two axes of rotation. These translations and rotations allow for precise alignment of the sample, the measurement of rocking curves by changing the incidence angle, and the access of the zone axes at different azimuthal angles; the angular precision is 0.005°. The laser fluence at the specimen was measured by imaging the beam profile and determining the Gaussian spot profile (3 mm by 0.24 mm for the full widths at half-maximum (FWHM)). Within the experimental repetition period of 1 ms, the sample at room temperature fully recovers to the initial ground state. This recovery was confirmed by observing no change in the diffraction patterns whether recorded at negative delay time (an effective 1-ms delay) or without the excitation. The observed changes by femtosecond (fs) excitation, therefore, reveal the nonequilibrium dynamics without contributions from static heating.

Text

The vertical and horizontal diffraction profiles at different delay times were fitted with a pseudo-Voigt function and a nearly constant background to extract the temporal evolution of the Bragg spot positions, intensities, widths (Fig. S2B) (*S5*). Because of the high signal-to-noise ratio, the *c*-axis expansion (deduced from the spot vertical position) can be determined to an accuracy of 0.007%; the diffraction intensity and peak width standard deviations are 0.75% and 1.2%, respectively (see the data in Figs. 3 and 4). Thus, the sensitivity of our UEC apparatus allows for detection of small diffraction changes as seen in Figs. 3B–3D for the low fluence cases.

The temporal evolution profiles of the lattice expansion, intensity and width can be fitted with the following formula $M(t)$ convoluted with our instrumental Gaussian response function (*S6*),

$$\begin{aligned} M(t) &= A\cdot\left[\exp\left(-\frac{t}{\tau_{decay}}\right)-\exp\left(-\frac{t}{\tau_{rise}}\right)\right]+A(0) \quad \text{for } t>0, \\ &= A(0) \quad \text{for } t<0 \end{aligned} \tag{S1}$$

where A and $A(0)$ are the amplitudes from the induced structural change and at negative times, respectively, and τ_{rise} and τ_{decay} are the time constants for the rise and decay parts of the change, respectively. For time-resolved electron diffraction of

condensed matter, however, the response function accounts for the diffraction difference following the optical excitation, since electrons can probe all structures.

All solid lines in Fig. 3 and all lines in Fig. 4 were obtained by such fitting. In Fig. S3, the fits of the temporal profiles of *c*-axis expansion in the low- and high-density nanowire arrays (Fig. 4C) are shown: τ_{rise} (low density) = 26±3 ps and τ_{rise} (high density) = 36±6 ps; τ_{decay} (low density) = 182±18 ps and τ_{decay} (high density) = 190±20 ps. Without losing the physical significance, we used the experimentally determined times at half maximum $\tau_{1/2}$ for further discussions. They are $\tau_{1/2}$ = 16 ps and $\tau_{1/2}$ = 32 ps for the low-density and high-density arrays, respectively.

Supporting figures

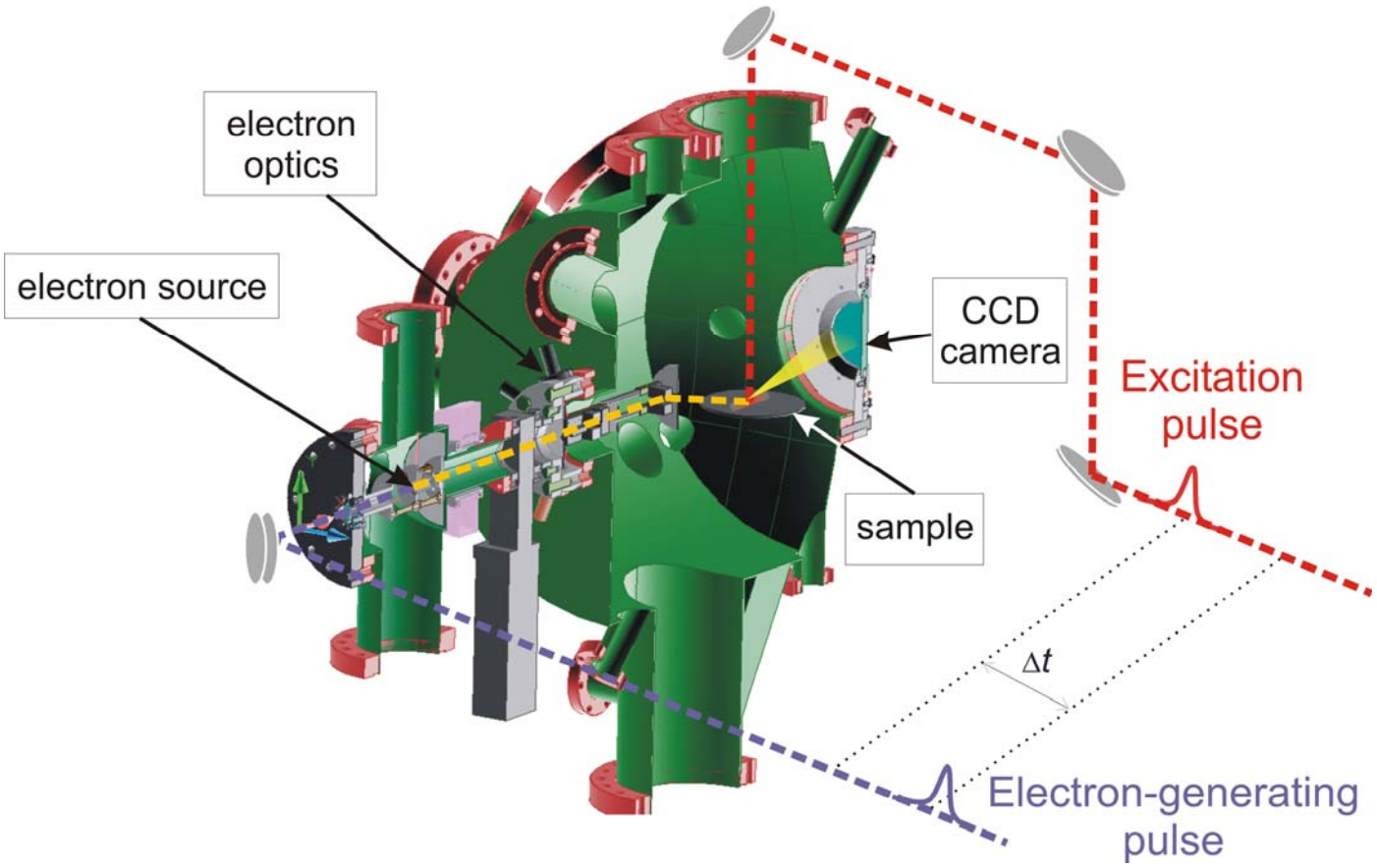

Fig. S1 Schematic of the UEC apparatus foscuing on the diffraction chamber and the integrated laser system. A cross-sectional view with paths of the optical excitation and electron-generating beams is shown along with electron optics and the CCD camera for detection (see Ref. *S7*).

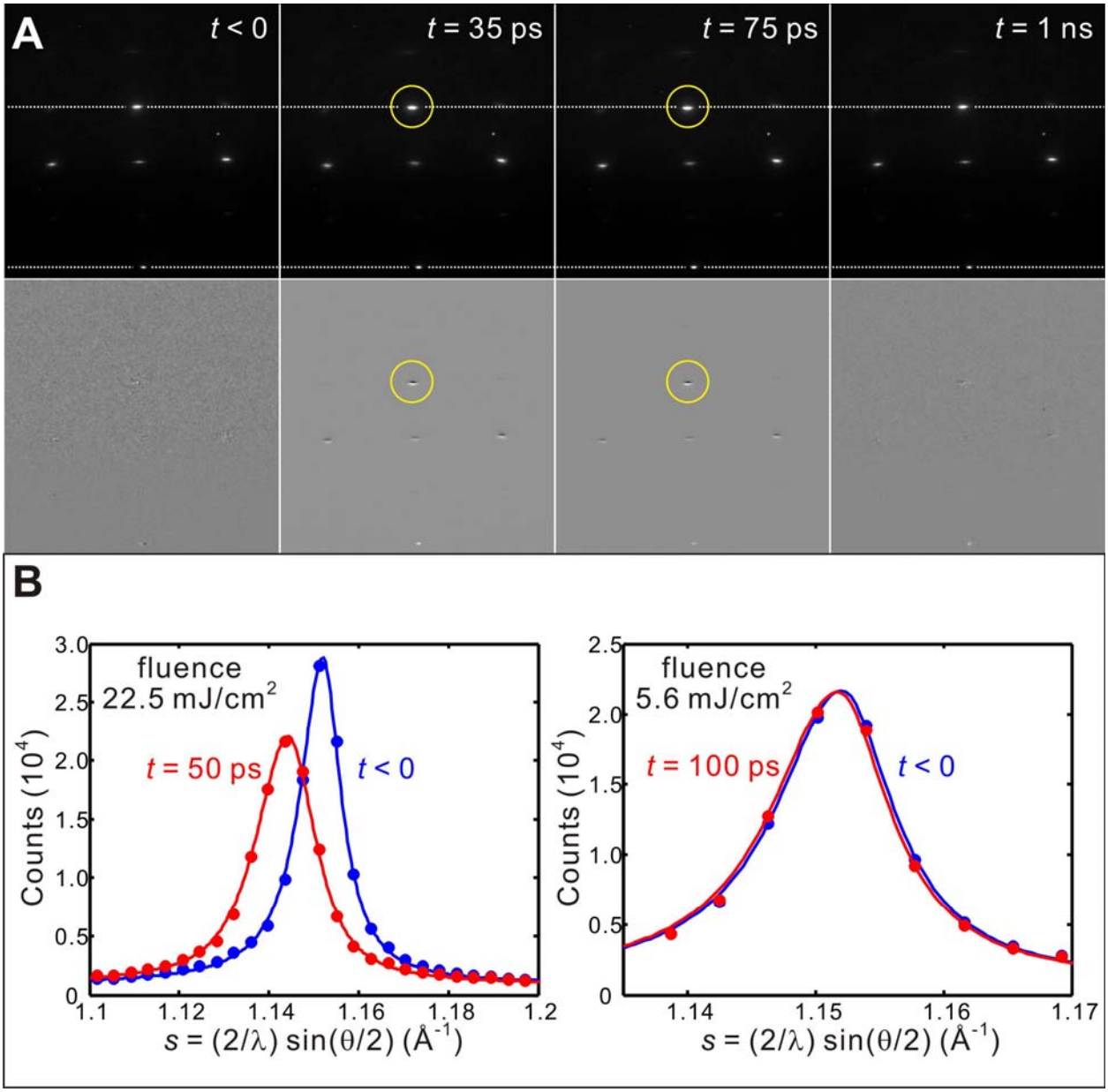

Fig. S2 (A) Diffraction images (upper panel) and differences (lower panel) at selective delay times. From the original images the movement of the (006) spot can be seen (yellow circles); the upper dashed line indicates its initial vertical position before excitation. Stationary nature of the (000) direct beam (referenced by the lower dashed line) is evident. The diffraction spots move downward at early times, as indicated by intensity losses (black) at the original positions and gains (white) at lower positions; at longer time the disappearance of diffraction difference signifies the recovery of the excited ZnO nanowires. (B) Vertical cross section of diffraction profiles for the (006) Bragg spot and the fits to pseudo-Voigt functions, at two selective delay times (blue and red), and at the highest (upper panel) and lowest (lower panel) fluences used. Here, s is the scattering vector and θ is the total deflection angle from the direct beam to the diffraction spot. Temporal evolution of the peak position, intensity and width was obtained from the fits at different delay times. The small shift of the diffraction peak at the lowest fluence well demonstrates the sensitivity of the UEC detection, as shown in Fig. 3B and discussed here.

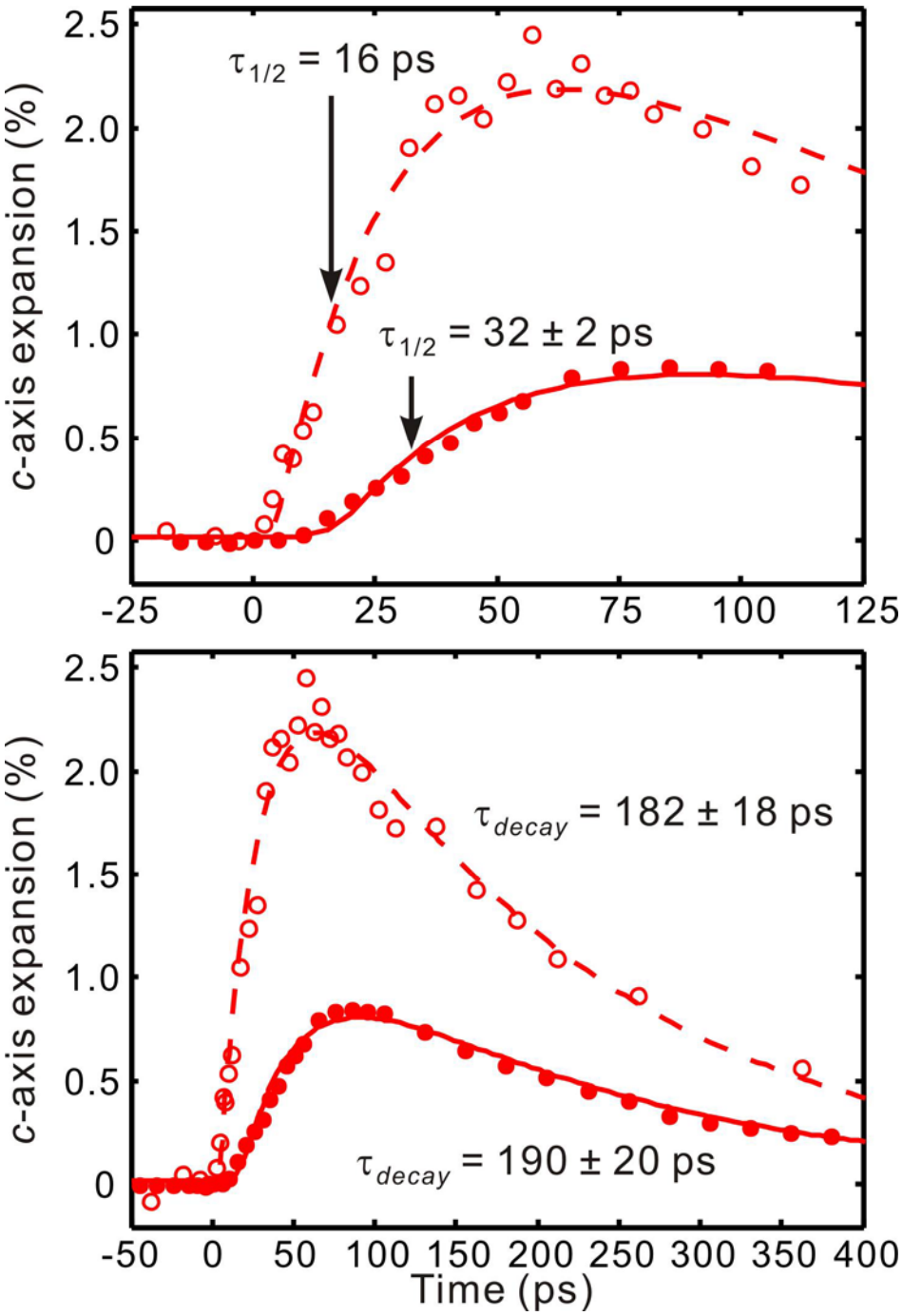

Fig. S3 Temporal evolution of the longitudinal expansion at short-time (upper panel) and long-time (lower panel) scales. Both the low-density (open circles and dashed line) and high-density (solid dots and line) nanowire arrays are displayed. The overall dynamics are similar, but the low-density array exhibits a faster rise and larger amplitude. The error bars given in the figure are the step size in the experiments (upper panel) and standard deviations from the fits (lower panel); because the rises are relatively slow (on the ps time scale), there was no need to record the entire profiles with fs resolution (*S2*, *S4*).

References:

S1. A. H. Zewail, *Annu. Rev. Phys. Chem.* **57**, 65 (2006) and references therein.

S2. P. Baum, D.-S. Yang, A. H. Zewail, *Science* **318**, 788 (2007).

S3. P. Baum, A. H. Zewail, *Proc. Natl. Acad. Sci. U.S.A.* **103**, 16105 (2006).

S4 F. Carbone, P. Baum, P. Rudolf, A. H. Zewail, *Phys. Rev. Lett.* **100**, 035501 (2008).

S5. D.-S. Yang, N. Gedik, A. H. Zewail, *J. Phys. Chem. C* **111**, 4889 (2007).

S6. S. Pedersen, A. H. Zewail, *Molecular Physics* **89**, 1455 (1996).

S7. N. Gedik, D.-S. Yang, G. Logvenov, I. Bozovic, A. H. Zewail, *Science* **316**, 425 (2007).